



HAL
open science

Near-Infrared-Luminescent Gold Nanoclusters Stabilized by End-Grafted Biocompatible Polymer Chains for Bioimaging

Bárbara Casteleiro, Fernande da Cruz-Boisson, Pierre Alcouffe, Sandra Pinto, José Gaspar Martinho, Marie-Thérèse Charreyre, José Paulo Sequeira Farinha, Arnaud Favier

► To cite this version:

Bárbara Casteleiro, Fernande da Cruz-Boisson, Pierre Alcouffe, Sandra Pinto, José Gaspar Martinho, et al.. Near-Infrared-Luminescent Gold Nanoclusters Stabilized by End-Grafted Biocompatible Polymer Chains for Bioimaging. *ACS Applied Nano Materials*, 2023, 6 (13), pp.11689-11698. 10.1021/ac-sanm.3c01665 . hal-04253783

HAL Id: hal-04253783

<https://cnrs.hal.science/hal-04253783v1>

Submitted on 23 Oct 2023

HAL is a multi-disciplinary open access archive for the deposit and dissemination of scientific research documents, whether they are published or not. The documents may come from teaching and research institutions in France or abroad, or from public or private research centers.

L'archive ouverte pluridisciplinaire **HAL**, est destinée au dépôt et à la diffusion de documents scientifiques de niveau recherche, publiés ou non, émanant des établissements d'enseignement et de recherche français ou étrangers, des laboratoires publics ou privés.

Near Infrared-Luminescent Gold Nanoclusters Stabilized by End-Grafted Biocompatible Polymer Chains for Bioimaging

Bárbara Casteleiro,^{a,b} Fernande Da Cruz-Boisson,^b Pierre Alcouffe,^b Sandra N. Pinto,^c José M.

Gaspar Martinho,^a Marie-Thérèse Charreyre,^b José Paulo Sequeira Farinha,^{a} Arnaud Favier^{b*}*

^a Centro de Química Estrutural, Institute of Molecular Sciences and Department of Chemical Engineering, Instituto Superior Técnico, University of Lisbon, P-1049-001 Lisbon, Portugal.

^b Université de Lyon, CNRS, Université Lyon 1, INSA Lyon, Université Jean Monnet, UMR 5223, Ingénierie des Matériaux Polymères, F-69621 Villeurbanne, France.

^c iBB-Institute of Bioengineering and Biosciences, i4HB—Institute for Health and Bioeconomy Instituto Superior Técnico, University of Lisbon, Av. Rovisco Pais, P-1049-001 Lisbon, Portugal.

ABSTRACT. Gold Nanoclusters (AuNCs) are an emerging class of nanomaterials for bioimaging, featuring high photostability, size-dependent luminescence, large Stokes shifts, long photoluminescence lifetimes, and good biocompatibility. However, when stabilized by small ligands, AuNCs exhibit a limited colloidal stability. Here, we report the synthesis of original “hairy” AuNCs with a diameter under 2 nm and NIR photoluminescence (for both 1-photon and 2-photon excitation), stabilized by biocompatible end-grafted poly(*N*-acryloyl morpholine) (PNAM) chains prepared by RAFT polymerization. The AuNCs synthesis was carried out directly in water in the presence of thiol-terminated PNAM-SH chains. Compared with AuNCs stabilized by small ligands, our PNAM-AuNCs exhibit much better colloidal stability (unchanged for more than two months), a 2-fold increase in photoluminescence lifetimes, and significantly enhanced quantum yields. Moreover, their properties could be successfully tuned using PNAM chains with molecular weights ranging from 3 000 to 11 000 g.mol⁻¹. These PNAM-AuNCs offer an excellent platform for the development of bioimaging probes without organic dyes.

KEYWORDS. Gold nanoclusters, RAFT polymerization, fluorescence bioimaging, NIR emitting probes, nanoparticle stabilization, DOSY NMR, chain-end grafting

INTRODUCTION

Gold Nanoclusters (AuNCs) are an emerging class of gold nanomaterials, with less than 300 Au atoms and dimensions below 2 nm, close to Fermi's wavelength of gold (0.5 nm).¹ These characteristics lead to quantum confinement effects, inducing the appearance of discrete energy levels and photoluminescence.² Moreover, since AuNCs are biocompatible and feature size-dependent photoluminescence, high photostability and large Stokes shifts, they offer an excellent alternative to organic dyes and quantum dots for bioimaging applications. These structures, synthesized for the first time in 1994 by Brust *et al.*,³ have been drawing attention in different fields, from chemistry and physics to biology and medicine.⁴⁻⁶

The surface ligands of AuNCs play a critical role on both their colloidal stability and their optical properties. The most studied ligands are thiol-containing small molecules,⁷⁻⁹ because the Au-S bond is as strong as the Au-Au bond, facilitating the AuNCs preparation.¹⁰ However, a disadvantage of this approach is the low colloidal stability of the resulting AuNCs and usually their low quantum yield (typically only ca. 0.1%).⁴ Although thiol ligands are still the most commonly used, AuNCs can also be prepared with ligands containing different gold interacting groups such as phosphines, alkynyls and selenolates,¹¹ or phenyl, carbonyl and amine groups.^{2, 12-15} Nonetheless, this kind of stabilization is usually less strong than that provided by thiol-containing molecules, leading to less stable AuNCs.¹⁶

A way to improve stabilization consists in embedding the AuNCs within macromolecular structures, especially proteins,^{8, 17-19} dendrimers²⁰⁻²¹ and other polymers.² Proteins interact with the gold core mostly via cysteine thiols but also via other groups, such as carboxylic and amine

groups.¹⁰ Due to their size, proteins provide steric stabilization to the AuNCs. In addition, higher photoluminescence quantum yields have been obtained with values generally between 5-10% (a study reporting values up to 56 %).²² Although protein-stabilized AuNCs are very promising for bioapplications, their preparation is limited to small quantities and requires a careful control of reaction conditions (such as pH, ionic strength and temperature) to maintain protein structure and activity.¹⁹ Dendrimers were one of the first templates used to embed AuNCs.^{20, 23} Like proteins, they can provide a good colloidal stabilization and host large numbers of AuNCs thanks to several gold interacting groups.²⁴⁻²⁵ AuNCs prepared within polyethylenimine (PEI) or poly(amidoamine) (PAMAM) dendrimers have shown good stability against aggregation and exhibited quantum yields that can reach values ranging from 10 to 70%, respectively for near infrared emitting Au₃₁NCs to smaller near-UV emitting Au₅NCs.²⁶ Nonetheless, large quantities of dendrimers are difficult to obtain as they require complex and costly synthesis.²⁷ Other multifunctional polymers with multiple gold interacting groups were then used to stabilize AuNCs, like random copolymers of oligo(ethylene oxide) methyl ether methacrylate and 2-(acetylthio)ethyl methacrylate synthesized by RAFT.²⁸ In this case, like for proteins and dendrimers, each (co)polymer chain may interact with several gold atoms of the same AuNC, or with several AuNCs.

In contrast, linear polymer chains with only one sulfur-containing end-group provide a different type of polymer-stabilized AuNCs,²⁹⁻³⁰ with several end-grafted chains at the surface ("hairy" AuNCs) (Scheme 1). In this situation, each polymer chain interacts with only one AuNC.

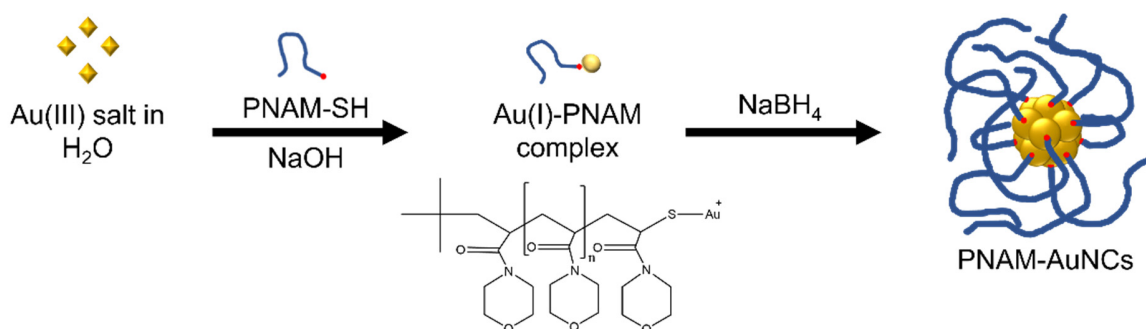


Figure 1. PNAM-AuNCs synthesis in water at room temperature. The Au(III) salt was first reduced to Au(I) by interaction with PNAM-SH in the presence of NaOH. Reduction to Au(0) by addition of NaBH₄ then resulted in the formation of hairy PNAM-AuNCs with a Au(0) core stabilized by end-grafted Au(I)-S-PNAM chains.

Examples of such gold nanoclusters stabilized by end-grafted polymer chains are quite rare, notably due to the synthetic challenge that represents the controlled introduction of a sulfur-containing group at a polymer chain-end. The first reported example involved the use of hydrophilic polymethacrylate chains bearing a thioether/thiol end-group, synthesized by conventional radical polymerization in the presence of irreversible thiol transfer agents.²⁹ However, this polymerization process does not provide control over molecular weight, size dispersity and chain-end functionalization efficiency. A few studies also reported the stabilization of AuNCs with thiol-terminated (generally lipoic acid) PEG chains.³¹⁻³² The resulting polymer-stabilized AuNCs exhibited quantum yields in the range of 2 to 14%,^{31, 33} high colloidal and photophysical stability, and were successfully applied for *in cellulo* bioimaging.³² The use of end-grafted polymer chains as AuNC macro-ligands offers better control as well as a simpler alternative to dendrimers and proteins, while providing similar stabilization.

Our approach here was to stabilize AuNCs with thiol-terminated chains synthesized by Reversible Addition-Fragmentation chain Transfer (RAFT) polymerization. The RAFT process is especially well-suited to produce polymer chains with a sulfur-containing end group (from the RAFT chain transfer agent) that can be easily converted into a thiol.³⁴⁻³⁵ Moreover, the chains have a controlled molecular weight and a low size dispersity. End-grafting RAFT polymers thus shows great promises to functionalize the surface of different types of gold nanostructures. Many examples have been reported with gold nanoparticles (AuNPs)³⁶ but very little with gold nanoclusters (AuNCs). To the best of our knowledge, only one report investigated the synthesis of AuNCs stabilized by a mixture of a PEO-PNIPAM-SH block copolymer (previously synthesized by RAFT) and small thiol ligands (lipoic acid).³³ The resulting thermosensitive AuNCs were then self-assembled into highly luminescent micelles.

In this study, RAFT polymerization was used to synthesize poly(*N*-acryloyl morpholine) (PNAM) chains, a biocompatible and fully water-soluble polymer,³⁷⁻³⁸ that can be modified to introduce other functionalities, such as bio-targeting.³⁹⁻⁴⁰ PNAM-stabilized-AuNCs were easily prepared directly in aqueous medium at room temperature. Their colloidal stability over time was investigated as well as their photoluminescence quantum yield, that was found to depend on the molecular weight of the thiol-terminated PNAM-SH chains. The resulting PNAM-AuNCs showed very promising results for (NIR) bioimaging, featuring high Stokes shifts and high photoluminescent lifetimes.

EXPERIMENTAL SECTION

Materials. Gold(III) chloride trihydrate ($\text{HAuCl}_4 \cdot 3\text{H}_2\text{O}$, $\geq 99.9\%$, Sigma-Aldrich), sodium hydroxide (NaOH, Carlo Erba) and sodium borohydride (NaBH_4 , $>98.5\%$, Sigma-Aldrich) were used as received. Deionized water used for synthesis was generated by a Millipore Milli-Q system (Millipore - Merck).

PNAM synthesis. Thiol-terminated poly(*N*-acryloyl morpholine) homopolymers (PNAM-SH) were synthesized according to a previously described procedure.³⁴⁻³⁵ RAFT polymerization using tert-butyl dithiobenzoate (tBDB) as control agent was followed by aminolysis of the ω -chain-end in the presence of aminoethyl morpholine (Figure S1).³⁵

AuNCs synthesis.

MHA-AuNCs. 6-Mercaptohexanoic acid-capped gold nanoclusters (MHA-AuNCs) were synthesized as previously reported.⁴¹⁻⁴²

3k-PNAM-AuNCs. An aqueous solution of 3k-PNAM-SH (12.9 mL, 1.9 mM, 24.3 μmol , 1.96 eq.) was added to a HAuCl_4 aqueous solution (498 μL , 24.9 mM, 12.4 μmol , 1 eq.) stirred in a water bath set at 27°C. NaOH (508 μL , 1.09 M, 0.55 mmol, 44.6eq.) was added, followed dropwise by a freshly prepared NaBH_4 solution in 0.2M NaOH (244 μL , 0.1 M, 0.24 μmol , 2.10 eq.). After 1h, 366 μL (3.15 eq., 0.37 μmol) of the same NaBH_4 solution (cooled down to 0°C before addition) was added and the mixture was stirred at 27°C for 2h. The final brown dispersion was stored at room temperature.

6k-PNAM-AuNCs and 11k-PNAM-AuNCs. Synthesis was similar to that of 3k-PNAM-AuNCs, except for the addition of NaBH_4 solution which was done in only 1 step (2.02 eq. for 6k-PNAM-AuNCs and 1.73 eq. for 11k-PNAM-AuNCs, added dropwise). The final mixture was stirred for 3h at 27°C.

Purification of PNAM-AuNCs. The AuNCs aqueous dispersions were purified by ultrafiltration against deionized water with molecular weight cut-off (MWCO) membranes from 3 000 g mol⁻¹ to 50 000 g mol⁻¹ as indicated (regenerated cellulose, Amicon Ultra, Millipore-Merck). Low MWCO (3 000 g mol⁻¹, PNAM being retained by the membrane) could be used to perform solvent exchange, remove salts and concentrate the aqueous dispersions. Higher MWCOs (10 000 g mol⁻¹ and 50 000 g mol⁻¹) were used to also remove the free PNAM chains.

Analytical techniques.

Size exclusion chromatography with multi-angle laser light scattering detection (SEC-MALLS). SEC-MALLS was performed in chloroform with a Mixed-C PL gel column (5 µm pore size) and a LC-6A Shimadzu pump (1 mL min⁻¹). Online double detection was provided by a differential refractometer (Waters DRI 410) and a MiniDAWN TREOS three-angle (46°, 90°, 133°) light scattering detector (Wyatt Technologies) operating at 658 nm. Analyses were run by injection of polymer solutions (3 g L⁻¹, 70 µL). The specific refractive index increment (dn/dc) of PNAM in chloroform (0.130 mL g⁻¹) was previously determined with an NFT-Scan interferometer operating at 633 nm. The molecular weight distribution data were obtained with the Wyatt ASTRA SEC/LS software package.⁴³

Nuclear Magnetic Resonance (NMR). ¹H and ¹H DOSY NMR experiments were recorded using a Bruker AVANCE III Spectrometer operating at 400.13 MHz.

The spectrometer was equipped with a 5 mm Z-gradients BBFO+ probe.³⁸ The samples prepared in water were transferred to deuterated water (D₂O) and deionized by ultrafiltration (3 000 g mol⁻¹ MWCO, 6 cycles). Spectra were acquired using the Bruker LEDBPGP2S⁴⁴ pulse program (stimulated echo sequence with bipolar gradient pulses). The gradient pulse length δ was optimized to each sample and varied between 1000 and 5000 µs. The diffusion delay was set to 100 ms. For

all experiments, gradients were linearly sampled from 0.978 G cm⁻¹ to 47.921 G cm⁻¹ in 40 points and the gradient pulses were smooth-square shaped (SMSQ10.100). Sixty-four scans were acquired on 16k data points (2.4 s recycle time). Fourier transform was applied to the free induction decays (FIDs) with 2 Hz Lorentzian line-broadening using the TopSpin software (Bruker) with automatic baseline correction. For each gradient strength value, the experimental signal amplitude (I) of a NMR resonance is given by the Stejskal-Tanner equation (1).⁴⁵

$$I = I_0 e^{-D\gamma^2 g^2 \delta^2 (\Delta - \frac{\delta}{3} - \frac{\tau}{2})} \quad (1)$$

Where I_0 is the reference amplitude (at zero gradient), D the diffusion coefficient, γ the gyromagnetic ratio of the observed nucleus, τ the time between the bipolar gradient pulses, g the gradient strength, δ the gradient pulse length, and Δ the diffusion time. The multi-exponential fitting of the Stejskal-Tanner curves was processed to determine the diffusion coefficients using Dynamic Center software that is able to distinguish between the different compounds of a complex mixture with overlapping signals. 2D ¹H DOSY NMR maps were obtained using the TopSpin software (Bruker).

Photoluminescence and UV-vis absorption spectra. Routine analyses were performed with a microplate reader (BioTek, Gen4 software) on samples without filtration or dilution (100 μL/well).

UV-Vis absorption spectra were recorded on a UV-660 UV-Vis spectrophotometer (JASCO International, Tokyo, Japan) with a double monochromator and photomultiplier detector for high resolution, using a Peltier temperature controller. Fluorescence spectra were recorded in right-angle geometry on a Horiba-Jobin Yvon Fluorolog 3-22 spectrofluorimeter equipped with a xenon lamp of 450 W. The software used was FluorEssence®. The raw samples were analyzed without further dilution at room temperature, using 0.5 cm optical path length quartz cell. The fluorescence

quantum yields were determined by the reference method using a Coumarin 102 solution in absolute ethanol (0.02%wt; $\Phi = 0.764$, $\lambda_{\text{exc}} = 350$ nm; $400 \text{ nm} < \lambda_{\text{em}} < 600$ nm) as the standard.⁴⁶

Time-resolved fluorescence. Fluorescence decay curves were recorded in 5 mm optical path length quartz cuvettes by time-correlated single photon counting (TCSPC) technique. A diode-pumped solid state mode-locked Nd:YVO₄ laser (Vanguard, Spectra Physics) was used, delivering 2W of 532 nm light at a repetition rate of 76 MHz and pulse duration of ~ 12 ps, that synchronously pumped a cavity-dumped dye lasers (701-2, Coherent, delivering 5-6 ps pulses with ~ 40 nJ pulse at 3.4 MHz) working with rhodamine 6G (Rh 6G, 560-610 nm). The laser emission is doubled by a BBO crystal delivering pulses at 300 nm, with a repetition rate of 152 kHz. Intensity decay measurements were recorded with the emission polarizer set at the magic angle (54.7°) relative to the vertical polarized excitation light. The emission light was passed through a depolarizer before reaching the Jobin-Yvon iHR320 monochromator (grating of 100 lines/mm, bandwidth 15-20 nm). The fluorescence was detected by a B&H PMC-100-02 photomultiplier in photon counting mode, with the pulses recorded by the multiscaler (MSA 300 from B&H) with 5 ns resolution. No less than 20 000 counts were accumulated at the maximum channel. Alternatively, a Delta Flex fluorescence lifetime spectrometer (Horiba scientific, USA) equipped with a 450 nm Delta diode excitation source was used to measure the fluorescence decay curves, which were analyzed using the TRFA Data Processor Advanced (Scientific Software Technologies Center, Belarusian State University).⁴⁷

Two-photon absorption (TPA). The TPA spectra were determined by two-photon induced fluorescence (TPF) using as excitation source a Ti:sapphire laser (Tsunami BB, Spectra-Physics, 710-990 nm, 1.7 W, 100 fs, 82 MHz). The emission upon two-photon absorption was measured within a narrow wavelength bandwidth centered at 580 nm selected by the H20Vis Jobin Yvon

monochromator placed at the entrance of a PMC-100-4 photomultiplier tube (Becker and Hickl GmbH). The integrated intensity over the entire emission band was extrapolated using the emission spectrum corrected by the detector sensitivity.

Matrix-assisted laser desorption ionization time-of-flight mass spectrometry (MALDI-TOF MS). MALDI-TOF spectra were acquired with a Voyager-DE PRO (AB Sciex, Framingham, MA) equipped with a nitrogen laser line at 337 nm. Anionic ions were accelerated to a final potential of 20 kV. Mass spectra were the sum of 300 shots, and an external mass calibration was used (a mixture of peptides from Sequazyme™ standards kit, AB Sciex). Instrumental mass accuracy is 0.008% for the reflectron-mode analyses. Samples were prepared by dissolving PNAM-SH in water at a concentration of 10 g L⁻¹. The matrix was sinapic acid (3,5-Dimethoxy-4-hydroxycinnamic acid, Sigma-Aldrich), used without further purification and dissolved in water/acetonitrile 70/30 v/v (10 g L⁻¹). Matrix and polymer solutions were mixed at a 9:1 v/v ratio. Then, 1 μL of the mixture was deposited and dried onto the MALDI sample plate.³⁵

High resolution transmission electron microscopy (HR-TEM). HR-TEM was used to characterize the AuNCs in a JEOL2100F TEM working at the accelerating voltage of 200 kV. 1 μL of raw sample was deposited onto an ultrathin carbon film coated on a copper grid (ref.CF400-CU-UL, EMS). The excess solution was carefully blotted off using filter paper and the grid was air-dried at room temperature. The HR-TEM images were analyzed with ImageJ software and the average AuNC size was determined from 172, 179 and 78 nanoclusters for 3k-PNAM-AuNCs, 6k-PNAM-AuNCs and 11k-PNAM-AuNCs, respectively.

Confocal and two-photon fluorescence microscopy. All measurements were performed on a Leica TCS SP5 (Leica Microsystems CMS GmbH, Mannheim, Germany) inverted confocal microscope (DMI600). Excitation lines (Argon or He-Ne laser) were focused on the sample by an

apochromatic water immersion objective (63x, NA 1.2; Zeiss, Jena Germany). A 111.4 μm diameter pinhole positioned in front of the image plane blocked out-of-focus signals. Two-photon excitation was performed using the same set-up coupled to a Ti:sapphire laser (Mai Tai, Spectra-Physics, Darmstadt, Germany) as the excitation source delivering short pulses (width around 100 fs at 780 nm). The images were analyzed using ImageJ software.

In cellulo evaluation.

HeLa cells were purchased from ECACC (European Collection of Authenticated Cell Cultures). The cells were cultured in Dulbecco's Modified Eagle Medium, DMEM (GIBCO™), supplemented with 10% fetal bovine serum (FBS, GIBCO™) and 1% penicillin/streptomycin (GIBCO™) and maintained in a humid atmosphere with 5% CO₂ at 37 °C. The cells were maintained with routinely subcultures (using TrypLE Express without phenol red, GIBCO™, for chemical detaching) and counted with a Neubauer chamber. The cells were incubated with AuNCs for 4h. Then, the commercial membrane marker WGA-AlexaFluor 633® was added for 15 minutes according to the instructions from the supplier (Thermo Fisher Scientific). After completing the labeling protocol, the unbound dyes were removed by washing the cells with PBS.

RESULTS AND DISCUSSION

Near infrared (NIR) emitting AuNCs were prepared using biocompatible poly(*N*-acryloyl morpholine) (PNAM) chains, synthesized by RAFT polymerization with very low size dispersity.³⁴ Aminolysis of the dithiobenzoate group at the chain-end (resulting from the RAFT chain transfer agent) resulted in a thiol group that can be used to prepare PNAM-stabilized gold nanostructures (Scheme 1).³⁶

Synthesis of PNAM-AuNCs.

PNAM-SH samples with increasing number-average molecular weights (M_n) of 3, 6 and 11 kg.mol⁻¹ were prepared using a previously optimized procedure (Figure S1 in ESI).³⁵ First, PNAM chains with a dithiobenzoate ω -end-group (PNAM-DB) were synthesized by RAFT polymerization. The average molecular weights and low molecular weight dispersity (\mathcal{D}) were confirmed by SEC-MALLS (Figure S2) and ¹H NMR (Figure S3) (Table 1). After aminolysis of the dithiobenzoate into a thiol end-group, the chains were characterized by MALDI-TOF-MS, that confirmed the very efficient chain-end functionalization (Figure S4). The resulting PNAM-SH homopolymers were then used as ligands for the synthesis of PNAM-stabilized gold nanoclusters (PNAM-AuNCs) directly in aqueous medium, at room temperature (Figure 1).

Table 1. ^1H NMR and SEC-MALLS characterization of the PNAM homopolymers before aminolysis.

Polymer	SEC-MALLS		NMR
	M_n (g.mol $^{-1}$)	D	M_n (g.mol $^{-1}$)
3k-PNAM-DB	3 000	1.04	3 100
6k-PNAM-DB	5 800	1.04	5 600
11k-PNAM-DB	11 200	1.02	10 000

The PNAM-AuNCs synthesis was adapted from the Brust method in which the gold salt is solubilized in an aqueous phase and the ligand in an organic phase, leading to the formation of the AuNCs in the organic phase.³ However, when water-soluble ligands are used, such as 6-mercaptohexanoic acid (MHA),⁴¹ the synthesis of AuNCs can be performed directly in water at room temperature, a more sustainable route that does not require the use of phase transfer agents (often unsuitable for biomedical applications). Since the PNAM-SH macroligands are fully water-soluble, we set-up a process in water similar to the one using MHA.⁴¹ PNAM-SH chains were added to Au(III) salt, reducing the Au(III) to Au(I) and forming Au(I)-S-PNAM complexes (Figure 1). The change in the gold oxidation state was detected by the color change of the aqueous solution (yellow to colorless) upon addition of PNAM-SH.¹⁵ This process was accelerated by the addition of a NaOH solution,¹⁵ which facilitates the etching by PNAM-SH. In the last step, addition of NaBH₄ led to the partial reduction of Au(I) to Au(0), to form the Au(0) core of the AuNCs, stabilized by several Au(I)-S-PNAM chains at the periphery.⁴⁸ During this step, the color changed again from colorless to brown over 3h. The sample solution was stored at room temperature, remaining visually stable with no detected sedimentation.

Several PNAM-SH homopolymers of increasing molecular weights (3k, 6k and 11k, Table 1) were used for the synthesis of PNAM-AuNCs, keeping the PNAM-SH: Au molar ratio constant. For longer PNAM chains, stable PNAM-AuNCs could be obtained for lower NaBH₄: Au molar ratio (using less reducing agent). This indicated that the increase in PNAM chain-length improved AuNCs stabilization.

PNAM-AuNCs size characterization.

The determination of the size of the PNAM-AuNCs was challenging. Due to the very small size of the AuNCs, characterization by either Dynamic Light Scattering (DLS) or Nanoparticle Tracking Analysis (NTA) were not fully reliable. On the other hand, although MALDI-TOF MS has been previously used for the determination of the average molecular weight (MW) of AuNCs stabilized by small ligands,⁴⁹⁻⁵⁰ we could not detect even the 3k-PNAM-AuNCs by this technique, probably because the MW of polymer-stabilized AuNCs was too high. Indeed, by assuming an Au₂₅(PNAM)₁₈ structure (the most common and stable number of gold atoms/ligands AuNCs), the MW of 3k-PNAM-AuNCs should be around 60 000 g.mol⁻¹. Finally, by using HR-TEM and ¹H DOSY NMR we could determine the PNAM-AuNCs core diameter and hydrodynamic diameter, respectively (Table 2).

The average diameter of the Au core for each PNAM-AuNCs sample was between 1.5 and 2.0 nm (Figures 2A to 2C, and 2E), comparable to that of AuNCs stabilized with small thiol ligands (MHA-AuNCs, 1.9 ± 0.4 nm, Table 2) as well as previously reported values (1.6 ± 0.3 nm).⁵¹ HR-TEM also brought confirmation about the characteristic Au crystalline structure of the core. It was clearly observed for 3k-PNAM-AuNCs (Figure 2D), while, for higher molecular weight PNAM

chains, the contrast was lower due to the larger polymer shell (the polymer itself being not dense enough to be imaged at such high voltage). The obtained gold atom spacing was 0.24 ± 0.01 nm, in agreement with the lattice spacing for the (111) planes of Au nanoparticles.⁵²

Table 2. Characterization by HR-TEM and ^1H DOSY NMR of the size of the PNAM-AuNCs and MHA-AuNCs, and their corresponding linear optical properties (Emission quantum yield Φ , wavelengths at maximum excitation $\lambda_{\text{exc max}}$ and emission $\lambda_{\text{em max}}$ and lifetime τ).

Sample	Au core diameter (nm)	Hydrodynamic diameter (nm)	Linear optical properties			
	HR TEM	^1H DOSY NMR	Φ (%)	$\lambda_{\text{exc max}}^{\text{a}}$ (nm)	$\lambda_{\text{em max}}^{\text{b}}$ (nm)	τ (μs)
3k-PNAM-AuNCs	2.0 ± 0.4	5.4 ± 0.5	4.9 ± 0.5	326	716	1.2
6k-PNAM-AuNCs	1.8 ± 0.3	9.3 ± 0.3	6.0 ± 0.9	316	704	1.3
11k-PNAM-AuNCs	1.5 ± 0.3	15 ± 1	12 ± 1	364	711	2.2
MHA-AuNCs	1.9 ± 0.4	3.7	0.05	350	800	0.4

^a $\lambda_{\text{em}} = 720$ nm (except for MHA-AuNCs where $\lambda_{\text{em}} = 800$ nm); ^b $\lambda_{\text{exc}} = 320$ nm (except for MHA-AuNCs where $\lambda_{\text{exc}} = 450$ nm).

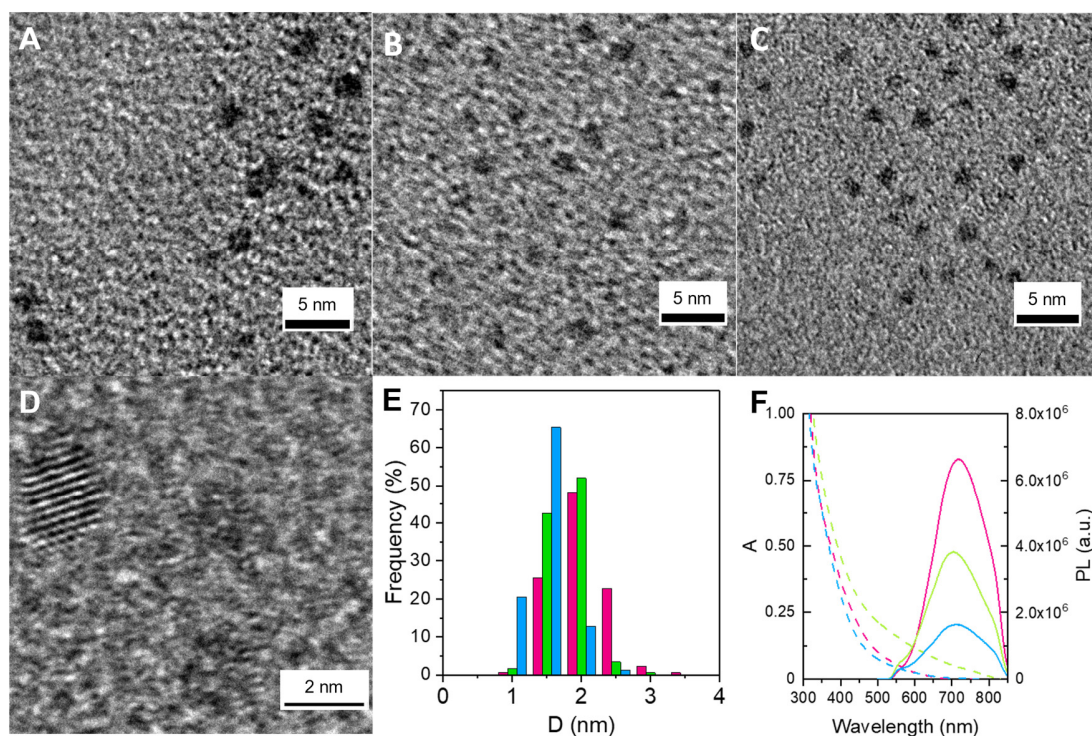


Figure 2. HR-TEM images (scale bar 5 nm) of 3k-PNAM-AuNCs (A), 6k-PNAM-AuNCs (B) and 11k-PNAM-AuNCs (C). Zoomed HR-TEM image (scale bar 2 nm) on the gold core crystalline structure of 3k-PNAM-AuNCs (D). (E) Distribution of the gold core diameter measured from HR-TEM images for 3k-PNAM-AuNCs (pink), 6k-PNAM-AuNCs (green) and 11k-PNAM-AuNCs (blue). (F) UV-vis absorption spectra (dashed lines) and photoluminescence spectra (continuous lines, $\lambda_{exc} = 320$ nm excitation) of 3k-PNAM-AuNCs (pink), 6k-PNAM-AuNCs (green) and 11k-PNAM-AuNCs (blue).

The hydrodynamic diameter of each PNAM-AuNC sample was calculated from the diffusion coefficient measured by ^1H DOSY NMR. For the ^1H DOSY NMR experiments, the PNAM-AuNCs samples were previously transferred into deuterium oxide (D_2O) and desalted by ultrafiltration ($3\,000\text{ g}\cdot\text{mol}^{-1}$ MWCO). In these conditions, only the higher molecular weight

components, such as free PNAM chains and PNAM-AuNCs were retained. Due to the significant size difference between the PNAM chains in solution and the PNAM-stabilized AuNCs, their diffusion coefficients were substantially different. For example, the 2D- ^1H DOSY map obtained for the 3k-PNAM-AuNCs sample (Figure 3) showed two distinct sets of PNAM peaks, the first at a lower diffusion coefficient ($8.0 \times 10^{-11} \text{ m}^2 \text{ s}^{-1}$) corresponding to PNAM-AuNCs and the second ($15 \times 10^{-11} \text{ m}^2 \cdot \text{s}^{-1}$) corresponding to free PNAM chains in solution.

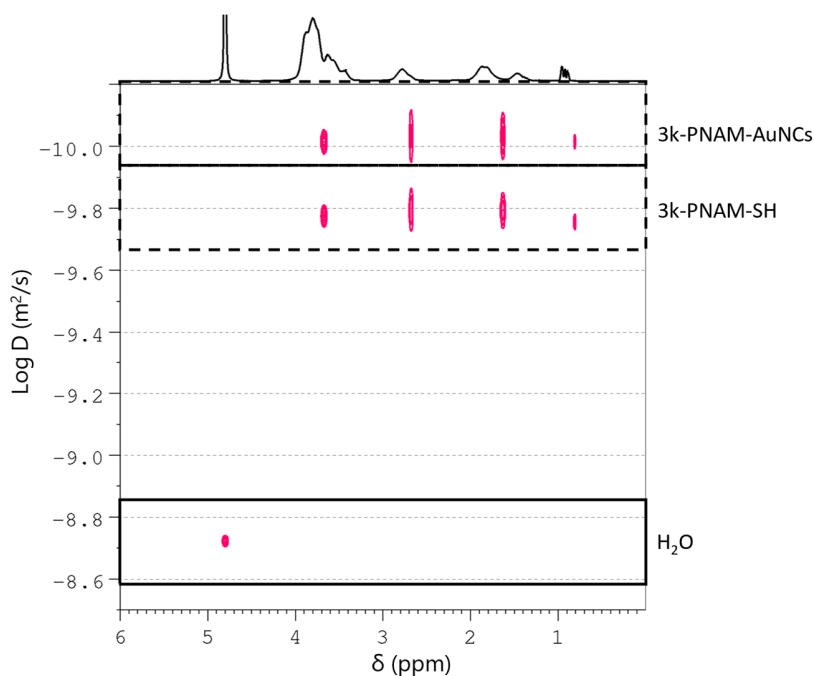


Figure 3. ^1H DOSY NMR 2D map for 3k-PNAM-AuNCs sample in D_2O .

The ^1H DOSY maps were similar for all the PNAM-AuNCs samples (Figure S5), with a decrease in the diffusion coefficient value for higher molecular weight PNAM chains, as expected (Table S1). The PNAM-AuNCs hydrodynamic diameter (D_h) was calculated by the Stokes-Einstein

equation (Eq.2) where D is the diffusion coefficient ($\text{m}^2 \cdot \text{s}^{-1}$), k_B the Boltzmann's constant, T the absolute temperature and η the viscosity (assuming that it is the same as the solvent).⁵³

$$D = \frac{k_B T}{3\pi\eta D_h} \quad (2)$$

For higher PNAM molecular weights, D_h increased from ca. 4.9 nm (3k-PNAM-AuNCs) to 15 nm (11k-PNAM-AuNCs) (Table 2). The higher D_h values of PNAM-AuNCs compared to that of MHA-AuNCs (3.7 nm, Figure S6) were expected due to the increase in the ligand size (Table 2). Interestingly, the D_h value for our MHA-AuNCs was higher than the one reported in the literature (2.7 nm, also by ^1H DOSY NMR), but corresponding to MHA-AuNCs produced via a different protocol, using MHA ligand in its more hydrophobic protonated form.⁵¹

Analysis of the ^1H DOSY 2D maps indicated the presence of PNAM chains bound to the AuNCs or free in solution, regardless of the polymer molecular weight. The average hydrodynamic diameter measured for the free PNAM chains tended to be higher than the values previously reported for similar PNAM-DB chains bearing a dithiobenzoate end-group,³⁸ indicating some contribution of PNAM-SH chains linked by a disulfide bond (PNAM-S-S-PNAM chains), formed by oxidation during DOSY NMR sample preparation.³⁵ This side reaction explains why the PNAM-AuNCs D_h values determined by DOSY (Table S1) were lower than the ones calculated by adding the HR-TEM diameter of the Au core and twice the DOSY hydrodynamic diameter of the free PNAM chains. Actually, the PNAM chains tethered at the gold surface probably adopt a more extended mushroom-like conformation than free chains in solution.

Optical Properties of PNAM-AuNCs.

Both the linear and non-linear optical properties of the PNAM-AuNCs were investigated by UV-vis absorption and photoluminescence spectroscopies. The UV-vis absorption spectra of the PNAM-AuNCs samples showed the characteristic λ^{-4} decay profile attributed to Rayleigh scattering, without discrete bands (Figure 2F). These spectra can be used to detect the possible aggregation of AuNCs into larger gold nanoparticles (AuNPs), which, unlike AuNCs, feature the characteristic surface plasmon resonance (SPR) band at ca. 520 nm for spherical AuNPs with diameters below 50 nm.⁵⁴ The fact that this SPR band was not observed for any of the PNAM-AuNCs samples confirmed the absence of gold particles with diameters larger than 2 nm.

The photoluminescence spectra of the PNAM-AuNCs exhibited a band in the red/NIR, with maximum emission wavelength at ≈ 710 nm for excitation at $\lambda_{\text{exc}} = 320$ nm (Figure 2F), explaining the red color of the dispersions observed under UV irradiation ($\lambda_{\text{exc}} = 365$ nm) (Figure S7). Only one emission band was observed regardless of the excitation wavelength from UV to green (280 nm to 450 nm, Figure S8), with the maximum emission intensity obtained for $\lambda_{\text{exc}} \approx 320$ nm (Table 2). Since the AuNCs photoluminescence is size dependent, these data indicated that the PNAM-AuNCs were monodisperse in size/number of Au atoms. The large Stokes shift was close to 350 nm (3.54 eV, 28 571.43 cm^{-1}) (Table 2 and Figure S8), leading to almost no overlap between the excitation and emission spectra. Such large Stokes shift values have already been reported for other AuNCs structures, such as AuNCs in nanosomes.⁵⁵ The PNAM-AuNCs emission ($\lambda_{\text{em(max)}} \approx 710$ nm) was slightly blue-shifted compared to gold nanoclusters stabilized with small thiol ligands prepared in similar conditions (MHA-AuNCs, $\lambda_{\text{em(max)}} \approx 800$ nm) (Table 2), probably due to the differences in ligand stabilization.⁵⁶

The photoluminescence quantum yields of the PNAM-AuNCs samples were determined using Coumarin 102 as reference ($\Phi = 76.4\%$ in ethanol),⁵⁷ both excited at 350 nm (Table 2). For the 3k-PNAM-AuNCs, the quantum yield was $\Phi = 4.9 (\pm 0.5) \%$, a 100-fold increase relative to that measured for MHA-AuNCs ($\Phi = 0.05\%$). This can be attributed to the change in the electronic environment around the gold core. The quantum yields of the different PNAM-AuNCs samples were all much higher than the ones reported in the literature for AuNCs stabilized by small thiol ligands, and in the same order of magnitude than those corresponding to AuNCs embedded within proteins⁵⁸⁻⁵⁹ and other polymers.^{30, 60} The quantum yield of the PNAM-AuNCs increased with the molecular weight of the PNAM-SH chains (Table 2). This is probably because the PNAM chains hinder the mobility of the Au(I) staple motifs at the AuNCs surface,⁶¹ decreasing the non-radiative deexcitation processes, and simultaneously acting to prevent the access of quenchers from solution, in particular molecular oxygen.⁶² This last effect of PNAM has been previously reported for organic dyes.³⁹

The photoluminescence decays of the PNAM-AuNCs samples (emission at 710 nm, upon excitation at 300 nm, Figure S9) were well fitted with a sum of 3-exponentials. Lifetime values in the range of microseconds were obtained, which increased with the PNAM molecular weight (Table S2). The average photoluminescence lifetimes for the PNAM-AuNCs samples (1000 to 2000 ns, Table 2) were similar to the values for AuNCs stabilized within proteins and other polymers^{30, 59} and 2- to 4-fold higher than the values obtained by us for MHA-AuNCs (ca. 500 ns) and reported in the literature for AuNCs stabilized by small ligands.⁶³ Time-resolved emission spectra (TRES) obtained from decays recorded by excitation at 450 nm showed that the spectra did not change along the decay curve, confirming that there was only one emitting species (Figure S10). The band at 700-770 nm is attributed to the surface states and probably involves charge

transfer processes between the ligands and the gold atoms.^{63,64} The increase of the average lifetime and the luminescence quantum yield with the PNAM chain-length (Figure S11) was mainly associated with the difference in quenching by molecular oxygen, not to changes in the arrangement of the gold core atoms or in the number of ligands per AuNC.⁶⁵ Nevertheless, this can also be partially due to the influence of electron-rich atoms (N and O) in the PNAM chain, which increase with the chain-length.¹¹ Indeed, it has been observed that ligands containing electron-rich atoms or groups of atoms enhance the AuNCs lifetime and luminescence quantum yield.⁶³

Finally, the PNAM-AuNCs could also be excited by two-photon absorption (TPA) in the NIR (Figure S13). The photoluminescence intensity (measured for emission at 685 nm and excitation at 850 nm) indeed exhibited a quadratic dependence with the power of the excitation intensity, with a slope close to 2 (Figure S12A). Both the photoluminescence and the excitation spectra showed that the non-linear optical properties were independent of the PNAM molecular weight (Figure S12B and S12C).

Stability of PNAM-AuNCs.

After preparation of the PNAM-AuNCs (3k, 6k and 11k), the samples were stored at room temperature without any purification. The stability of the 3k-PNAM-AuNCs over time was evaluated in terms of visual aspect, optical properties and ¹H DOSY NMR. The aqueous dispersion remained brown (Figure S7) for at least 24 months, with the color intensity slowly increasing with time. The formation of a white precipitate at the bottom of the flask, possibly corresponding to salts, was noticed after 7 weeks (no such precipitate was observed for desalted samples). The photophysical properties (UV-Vis absorption and photoluminescence) remained similar for a few

months. Only after 80 days, a weak SPR band appeared between 500 and 600nm on the UV-vis absorption spectrum (Figure S13, left column). This band witnessed the formation of few AuNPs (by irreversible aggregation of AuNCs). Only after 143 days, the photoluminescence intensity slightly decreased, with a red-shift of the maximum emission wavelength. These observations were probably related to the slow evolution of the 3k-PNAM-AuNCs into larger AuNCs. ^1H DOSY NMR analysis that reflects the overall size of the nanoparticles in dispersion confirmed an increase in the average hydrodynamic diameter (for the same sample but after ultrafiltration at day 0), from $D_h = 4.9$ nm to $D_h = 8.7$ nm after 71 days, and to $D_h = 14.9$ nm after 191 days (Figure S14). 6k-PNAM-AuNCs and 11k-PNAM-AuNCs samples with longer PNAM chains were even more stable. No SPR band appeared on the absorption spectra and no shift was observed in the photoluminescence band for 85 days (Figure S13, left column).

In conclusion, the PNAM-AuNCs samples exhibited a remarkable colloidal stability and no photodegradation for at least 2 months at room temperature, this stability increasing with the PNAM molecular weight.

***In cellulo* photoluminescence of PNAM-AuNCs.**

In the literature, AuNCs with different ligands and surface functionalization have been used to label cells and cell compartments.^{66,68} Although their biocompatibility has been demonstrated, the biological environment may lead to AuNCs destabilization.⁶⁹ In our case, the use of PNAM-SH chains as macroligand resulted in a significant improvement of the colloidal stability and optical properties of the resulting PNAM-AuNCs, both important characteristics for bioimaging applications. We thus evaluated the ability to image the PNAM-AuNCs *in cellulo* by confocal microscopy. The PNAM-AuNCs samples were first isolated from the free polymer by

ultrafiltration using high MWCO (10 000 and 50 000 g.mol⁻¹) and we checked that the purification step did not alter the sample properties (Figure S13, right column). NIR photoluminescence was maintained and no SPR band (resulting from irreversible aggregation into AuNPs) was observed on the UV-vis absorption spectra. The PNAM-AuNC samples were incubated 4 hours with HeLa cells and successfully imaged using either one-photon excitation at 458 nm (Figure 4) or two-photon excitation at 780 nm (Figure S15 and S16).

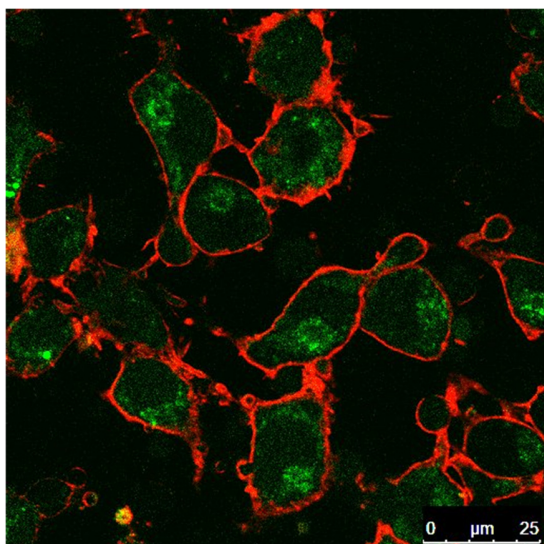


Figure 4. Merged confocal images of HeLa cells labeled with 6k-PNAM-AuNCs (4h incubation, $\lambda_{exc}=458$ nm, represented in green) and WGA-Alexa633 (plasma membrane marker, $\lambda_{exc}=633$ nm, represented in red). NIR-emitting 6k-PNAM-AuNCs were homogeneously distributed in the cytoplasm of the HeLa cells.

The PNAM-AuNCs were rapidly internalized and were clearly observed inside the cytoplasm of the cells. Cell uptake of AuNCs has indeed been shown to proceed mainly by endocytosis,⁴ thus leading to endosomal localization in the perinuclear region of the cells. The detected

photoluminescence intensity was relatively low. However, it was due to the low sensitivity of the confocal microscope detector, that strongly decreases above 690 nm (Figure S17). Nevertheless, the large Stokes shift of the PNAM-AuNCs (around 350 nm) is a strong advantage for optical microscopy. In addition, their long photoluminescence lifetimes and NIR emission are valuable features for bioimaging applications, such as time-gated fluorescence microscopy or deep tissue imaging.^{68,70}

CONCLUSIONS

Gold nanoclusters stabilized by end-grafted PNAM polymer chains prepared by RAFT polymerization (PNAM-AuNCs) were synthesized directly in aqueous medium at room temperature. The PNAM-AuNCs presented remarkable colloidal stability (up to 2 months at room temperature) in comparison with AuNCs stabilized by small ligands. Moreover, PNAM-AuNCs displayed NIR-photoluminescence, with quantum yields of *ca.* 12 % (much higher than those of small ligand-stabilized AuNCs, generally lower than 0.1%), and extended photoluminescent lifetimes of *ca.* 2.2 μ s. Their hydrodynamic diameter and optical properties were dependent on the PNAM molecular weight that can be controlled thanks to the RAFT process. Colloidal stability, quantum yield and photoluminescence lifetimes increased with PNAM chain-length. In addition, considering their large Stokes shift and the demonstrated possibility of both 1-photon and 2-photon excitation, our PNAM-AuNCs are highly promising tools for application in bioimaging without organic dyes.

ASSOCIATED CONTENT

Supporting Information. Complementary characterization of PNAM chains. Additional data about size, linear and non-linear optical properties, stability and *in cellulo* photoluminescence of PNAM-AuNCs. The following files are available free of charge.

AUTHOR INFORMATION

Corresponding Authors

* farinha@tecnico.ulisboa.pt

* arnaud.favier@univ-lyon1.fr

Notes

There are no conflicts to declare.

ACKNOWLEDGMENT

This work was supported by Fundação para a Ciência e a Tecnologia (FCT-Portugal) and COMPETE (FEDER) within projects PTDC/CTM-COM/1581/2021, UIDP/00100/2020 and LA/P/0056/2020. BC also thanks FCT for PhD grant PD/BD/137511/2018. This Portuguese/French binational collaborative work was also supported by Hubert Curien Partnership “PESSOA” program n°44648XM. We acknowledge Agnès Crépet (SEC-MALLS), Catherine Ladavière (MALDI-TOF MS), Carlos Fernandez-De Alba (DOSY NMR) from Laboratoire d’Ingénierie des Matériaux Polymères as well as the liquid chromatography and NMR platforms of Institut de Chimie de Lyon for their expertise and technical support. We also thank the Protein Science (Frédéric Delolme, SFR BioSciences (UMS3444-CNRS/US8-INSERM, UCBL, ENS de Lyon) and Electron Microscopy (CT μ , UCBL) technical facilities.

REFERENCES

- (1) Zhou, M.; Du, X.; Wang, H.; Jin, R. The Critical Number of Gold Atoms for a Metallic State Nanocluster: Resolving a Decades-Long Question. *ACS Nano* **2021**, *15*, 13980-13992. 10.1021/acsnano.1c04705
- (2) Casteleiro, B.; Martinho, J. M. G.; Farinha, J. P. S. Encapsulation of gold nanoclusters: stabilization and more. *Nanoscale* **2021**, *13*, 17199-17217. 10.1039/d1nr04939a
- (3) Brust, M.; Walker, M.; Bethell, D.; Schiffrin, D. J.; Whyman, R. Synthesis of thiol-derivatised gold nanoparticles in a two-phase Liquid-Liquid system. *J. Chem. Soc., Chem. Commun.* **1994**, 801-802. 10.1039/c39940000801
- (4) Zheng, Y.; Lai, L.; Liu, W.; Jiang, H.; Wang, X. Recent advances in biomedical applications of fluorescent gold nanoclusters. *Adv. Colloid Interface Sci.* **2017**, *242*, 1-16. 10.1016/j.cis.2017.02.005
- (5) Buceta, D.; Pineiro, Y.; Vazquez-Vazquez, C.; Rivas, J.; Lopez-Quintela, M. A. Metallic Clusters: Theoretical Background, Properties and Synthesis in Microemulsions. *Catalysts* **2014**, *4*, 356-374. 10.3390/catal4040356
- (6) Mathew, A.; Pradeep, T. Noble Metal Clusters: Applications in Energy, Environment, and Biology. *Part. Part. Syst. Charact.* **2014**, *31*, 1017-1053. 10.1002/ppsc.201400033
- (7) Ackerson, C. J.; Jadzinsky, P. D.; Kornberg, R. D. Thiolate Ligands for Synthesis of Water-Soluble Gold Clusters. *J. Am. Chem. Soc.* **2005**, *127*, 6550-6551. 10.1021/ja046114i
- (8) Sonia; Komal; Kukreti, S.; Kaushik, M. Gold nanoclusters: An ultrasmall platform for multifaceted applications. *Talanta* **2021**, *234*. 10.1016/j.talanta.2021.122623
- (9) Liu, Z.; Li, Y.; Kahng, E.; Xue, S.; Du, X.; Li, S.; Jin, R. Tailoring the Electron-Phonon Interaction in Au₂₅(SR)₁₈ Nanoclusters via Ligand Engineering and Insight into Luminescence. *ACS Nano* **2022**. 10.1021/acsnano.2c06586
- (10) Song, X.-R.; Goswami, N.; Yang, H.-H.; Xie, J. Functionalization of metal nanoclusters for biomedical applications. *Analyst* **2016**, *141*, 3126-3140. 10.1039/c6an00773b

- (11) Zhang, B.; Chen, J.; Cao, Y.; Chai, O. J. H.; Xie, J. Ligand Design in Ligand-Protected Gold Nanoclusters. *Small* **2021**, *17*, 2004381. 10.1002/sml.202004381
- (12) Ungor, D.; Dékány, I.; Csapó, E. Reduction of Tetrachloroaurate(III) Ions With Bioligands: Role of the Thiol and Amine Functional Groups on the Structure and Optical Features of Gold Nanohybrid Systems. *Nanomater.* **2019**, *9*, 1229.
- (13) Sun, Y.; Wang, D.; Zhao, Y.; Zhao, T.; Sun, H.; Li, X.; Wang, C.; Yang, B.; Lin, Q. Polycation-functionalized gold nanodots with tunable near-infrared fluorescence for simultaneous gene delivery and cell imaging. *Nano Res.* **2018**, *11*, 2392-2404. 10.1007/s12274-017-1860-4
- (14) Haesuwannakij, S.; Kimura, T.; Furutani, Y.; Okumura, K.; Kokubo, K.; Sakata, T.; Yasuda, H.; Yakiyama, Y.; Sakurai, H. The Impact of the Polymer Chain Length on the Catalytic Activity of Poly(N-vinyl-2-pyrrolidone)-supported Gold Nanoclusters. *Sci. Rep.* **2017**, *7*, 9579. 10.1038/s41598-017-10165-9
- (15) Zhu, M.; Lanni, E.; Garg, N.; Bier, M. E.; Jin, R. Kinetically Controlled, High-Yield Synthesis of Au₂₅ Clusters. *J. Am. Chem. Soc.* **2008**, *130*, 1138-1139. 10.1021/ja0782448
- (16) Qu, X.; Li, Y.; Li, L.; Wang, Y.; Liang, J.; Liang, J. Fluorescent gold nanoclusters: synthesis and recent biological application. *J. Nanomater.* **2015**, Art. 4. 10.1155/2015/784097
- (17) Ding, H.; Li, H.; Wang, X.; Zhou, Y.; Li, Z.; Hiltunen, J. K.; Shen, J.; Chen, Z. Expanding Toolbox of Imageable Protein-Gold Hybrid Materials. *Chem. Mater.* **2017**, *29*, 8440-8448. 10.1021/acs.chemmater.7b03011
- (18) Chevrier, D. M.; Chatt, A.; Zhang, P. Properties and applications of protein-stabilized fluorescent gold nanoclusters: short review. *J. Nanophotonics* **2012**, *6*. 10.1117/1.jnp.6.064504
- (19) Chen, L.-Y.; Wang, C.-W.; Yuan, Z.; Chang, H.-T. Fluorescent Gold Nanoclusters: Recent Advances in Sensing and Imaging. *Anal. Chem.* **2015**, *87*, 216-229. 10.1021/ac503636j
- (20) Kim, J. M.; Sohn, S. H.; Han, N. S.; Park, S. M.; Kim, J.; Song, J. K. Blue Luminescence of Dendrimer-Encapsulated Gold Nanoclusters. *Chem. Phys. Chem.* **2014**, *15*, 2917-2921. doi:10.1002/cphc.201402287

- (21) Vohs, J. K.; Fahlman, B. D. Advances in the controlled growth of nanoclusters using a dendritic architecture. *New J. Chem.* **2007**, *31*, 1041-1051. 10.1039/b616472m
- (22) El-Sayed, N.; Schneider, M. Advances in biomedical and pharmaceutical applications of protein-stabilized gold nanoclusters. *J. Mater. Chem. B* **2020**, *8*, 8952-8971. 10.1039/d0tb01610a
- (23) He, J.-A.; Valluzzi, R.; Yang, K.; Dolukhanyan, T.; Sung, C.; Kumar, J.; Tripathy, S. K.; Samuelson, L.; Balogh, L.; Tomalia, D. A. Electrostatic Multilayer Deposition of a Gold-Dendrimer Nanocomposite. *Chem. Mater.* **1999**, *11*, 3268-3274. 10.1021/cm990311c
- (24) Gröhn, F.; Bauer, B. J.; Akpalu, Y. A.; Jackson, C. L.; Amis, E. J. Dendrimer Templates for the Formation of Gold Nanoclusters. *Macromolecules* **2000**, *33*, 6042-6050. 10.1021/ma000149v
- (25) Ott, L. S.; Finke, R. G. Transition-metal nanocluster stabilization for catalysis: A critical review of ranking methods and putative stabilizers. *Coord. Chem. Rev.* **2007**, *251*, 1075-1100. 10.1016/j.ccr.2006.08.016
- (26) Zheng, J.; Zhang, C.; Dickson, R. M. Highly Fluorescent, Water-Soluble, Size-Tunable Gold Quantum Dots. *Phys. Rev. Lett.* **2004**, *93*, 077402. 10.1103/PhysRevLett.93.077402
- (27) Yu, Y.; Lin, C.; Li, B.; Zhao, P.; Zhang, S. Dendrimer-like core cross-linked micelle stabilized ultra-small gold nanoclusters as a robust catalyst for aerobic oxidation of α -hydroxy ketones in water. *Green Chem.* **2016**, *18*, 3647-3655. 10.1039/c6gc00010j
- (28) Adnan, N. N. M.; Ahmad, S.; Kuchel, R. P.; Boyer, C. Exploring the potential of linear polymer structures for the synthesis of fluorescent gold nanoclusters. *Mater. Chem. Front.* **2017**, *1*, 80-90. 10.1039/c6qm00109b
- (29) Wang, Z.; Tan, B.; Hussain, I.; Schaeffer, N.; Wyatt, M. F.; Brust, M.; Cooper, A. I. Design of Polymeric Stabilizers for Size-Controlled Synthesis of Monodisperse Gold Nanoparticles in Water. *Langmuir* **2007**, *23*, 885-895. 10.1021/la062623h
- (30) Deepagan, V. G.; Leiske, M. N.; Fletcher, N. L.; Rudd, D.; Tieu, T.; Kirkwood, N.; Thurecht, K. J.; Kempe, K.; Voelcker, N. H.; Cifuentes-Rius, A. Engineering Fluorescent Gold

Nanoclusters Using Xanthate-Functionalized Hydrophilic Polymers: Toward Enhanced Monodispersity and Stability. *Nano Lett.* **2021**, *21*, 476-484. 10.1021/acs.nanolett.0c03930

(31) Aldeek, F.; Muhammed, M. A. H.; Palui, G.; Zhan, N.; Mattoussi, H. Growth of Highly Fluorescent Polyethylene Glycol- and Zwitterion-Functionalized Gold Nanoclusters. *ACS Nano* **2013**, *7*, 2509-2521. 10.1021/nm305856t

(32) Oh, E.; Fatemi, F. K.; Currie, M.; Delehanty, J. B.; Pons, T.; Fragola, A.; Lévêque-Fort, S.; Goswami, R.; Susumu, K.; Huston, A. L.; Medintz, I. L. PEGylated Luminescent Gold Nanoclusters: Synthesis, Characterization, Bioconjugation, and Application to One- and Two-Photon Cellular Imaging. *Part. Part. Syst. Charact.* **2013**, *30*, 453-466. 10.1002/ppsc.201200140

(33) Hembury, M.; Beztsinna, N.; Asadi, H.; van den Dikkenberg, J. B.; Meeldijk, J. D.; Hennink, W. E.; Vermonden, T. Luminescent Gold Nanocluster-Decorated Polymeric Hybrid Particles with Assembly-Induced Emission. *Biomacromolecules* **2018**, *19*, 2841-2848. 10.1021/acs.biomac.8b00414

(34) Favier, A.; Charreyre, M. T. Experimental requirements for an efficient control of free-radical polymerizations via the reversible addition-fragmentation chain transfer (RAFT) process. *Macromol. Rapid Commun.* **2006**, *27*, 653-692. 10.1002/marc.200500839

(35) Gaillot, C.; Delolme, F.; Fabre, L.; Charreyre, M.-T.; Ladavière, C.; Favier, A. Taking Advantage of Oxidation to Characterize Thiol-Containing Polymer Chains by MALDI-TOF Mass Spectrometry. *Anal. Chem.* **2020**, *92*, 3804-3809. 10.1021/acs.analchem.9b05207

(36) Ceperaga, C.; Favier, A.; Lerouge, F.; Alcouffe, P.; Chamignon, C.; Lanoë, P.-H.; Monnereau, C.; Marotte, S.; Ben Daoud, E.; Marvel, J.; Leverrier, Y.; Andraud, C.; Parola, S.; Charreyre, M.-T. Fluorescent gold nanoparticles with chain-end grafted RAFT copolymers: influence of the polymer molecular weight and type of chromophore. *Polym. Chem.* **2016**, *7*, 6812-6825. 10.1039/c6py01625a

(37) Gorman, M.; Chim, Y. H.; Hart, A.; Riehle, M. O.; Urquhart, A. J. Poly(N-acryloylmorpholine): A simple hydrogel system for temporal and spatial control over cell adhesion. *J. Biomed. Mater. Res. Part A* **2014**, *102*, 1809-1815. 10.1002/jbm.a.34853

- (38) Chamignon, C.; Duret, D.; Charreyre, M.-T.; Favier, A. ¹H DOSY NMR Determination of the Molecular Weight and the Solution Properties of Poly(N-acryloylmorpholine) in Various Solvents. *Macromol. Chem. Phys.* **2016**, *217*, 2286-2293. 10.1002/macp.201600089
- (39) Relogio, P.; Bathfield, M.; Haftek-Terreau, Z.; Beija, M.; Favier, A.; Giraud-Panis, M.-J.; D'Agosto, F.; Mandrand, B.; Farinha, J. P. S.; Charreyre, M.-T.; Martinho, J. M. G. Biotin-end-functionalized highly fluorescent water-soluble polymers. *Polym. Chem.* **2013**, *4*, 2968-2981. 10.1039/c3py00059a
- (40) Duret, D.; Grassin, A.; Henry, M.; Jacquet, T.; Thoreau, F.; Denis-Quanquin, S.; Coll, J.-L.; Boturyn, D.; Favier, A.; Charreyre, M.-T. "Polymultivalent" Polymer-Peptide Cluster Conjugates for an Enhanced Targeting of Cells Expressing $\alpha v \beta 3$ Integrins. *Bioconjugate Chem.* **2017**, *28*, 2241-2245. 10.1021/acs.bioconjchem.7b00362
- (41) Yuan, X.; Zhang, B.; Luo, Z. T.; Yao, Q. F.; Leong, D. T.; Yan, N.; Xie, J. P. Balancing the Rate of Cluster Growth and Etching for Gram-Scale Synthesis of Thiolate-Protected Au₂₅ Nanoclusters with Atomic Precision. *Angew. Chem. Int. Ed.* **2014**, *53*, 4623-4627. 10.1002/anie.201311177
- (42) Casteleiro, B.; Ribeiro, T.; Mariz, I.; Martinho, J. M. G.; Farinha, J. P. S. Encapsulation of gold nanoclusters by photo-initiated miniemulsion polymerization. *Colloids Surf. A* **2022**, 129410. 10.1016/j.colsurfa.2022.129410
- (43) Berki, T.; Bakunts, A.; Duret, D.; Fabre, L.; Ladavière, C.; Orsi, A.; Charreyre, M.-T.; Raimondi, A.; van Anken, E.; Favier, A. Advanced Fluorescent Polymer Probes for the Site-Specific Labeling of Proteins in Live Cells Using the HaloTag Technology. *ACS Omega* **2019**, *4*, 12841-12847. 10.1021/acsomega.9b01643
- (44) Wu, D. H.; Chen, A. D.; Johnson, C. S. An Improved Diffusion-Ordered Spectroscopy Experiment Incorporating Bipolar-Gradient Pulses. *J. Magn. Reson., Series A* **1995**, *115*, 260-264. 10.1006/jmra.1995.1176
- (45) Stejskal, E. O.; Tanner, J. E. Spin Diffusion Measurements: Spin Echoes in the Presence of a Time-Dependent Field Gradient. *J. Chem. Phys.* **1965**, *42*, 288-292. 10.1063/1.1695690

- (46) Seybold, P. G.; Gouterman, M. Porphyrins: XIII: Fluorescence spectra and quantum yields. *J. Mol. Spectrosc.* **1969**, *31*, 1-13. 10.1016/0022-2852(69)90335-X
- (47) Digris, A. V.; Novikov, E. G.; Skakun, V. V.; Apanasovich, V. V.: Global Analysis of Time-Resolved Fluorescence Data. In *Fluorescence Spectroscopy and Microscopy: Methods and Protocols*; Engelborghs, Y., Visser, A. J. W. G., Eds.; Humana Press: Totowa, NJ, 2014; pp 257-277.
- (48) Wu, Z.; MacDonald, M. A.; Chen, J.; Zhang, P.; Jin, R. Kinetic Control and Thermodynamic Selection in the Synthesis of Atomically Precise Gold Nanoclusters. *J. Am. Chem. Soc.* **2011**, *133*, 9670-9673. 10.1021/ja2028102
- (49) Zhang, Y.; Shuang, S.; Dong, C.; Lo, C. K.; Paa, M. C.; Choi, M. M. F. Application of HPLC and MALDI-TOF MS for Studying As-Synthesized Ligand-Protected Gold Nanoclusters Products. *Anal. Chem.* **2009**, *81*, 1676-1685. 10.1021/ac8026349
- (50) Kouchi, H.; Kawasaki, H.; Arakawa, R. A new matrix of MALDI-TOF MS for the analysis of thiolate-protected gold clusters. *Anal. Meth.* **2012**, *4*, 3600-3603. 10.1039/c2ay26013a
- (51) Schuetze, B.; Mayer, C.; Loza, K.; Gocyla, M.; Heggen, M.; Epple, M. Conjugation of thiol-terminated molecules to ultrasmall 2 nm-gold nanoparticles leads to remarkably complex 1H-NMR spectra. *J. Mater. Chem. B* **2016**, *4*, 2179-2189. 10.1039/c5tb02443a
- (52) Wang, Y. Q.; Liang, W. S.; Geng, C. Y. Coalescence Behavior of Gold Nanoparticles. *Nanoscale Res. Lett.* **2009**, *4*, 684. 10.1007/s11671-009-9298-6
- (53) Salorinne, K.; Lahtinen, T.; Koivisto, J.; Kalenius, E.; Nissinen, M.; Pettersson, M.; Häkkinen, H. Nondestructive Size Determination of Thiol-Stabilized Gold Nanoclusters in Solution by Diffusion Ordered NMR Spectroscopy. *Anal. Chem.* **2013**, *85*, 3489-3492. 10.1021/ac303665b
- (54) Amendola, V.; Pilot, R.; Frasconi, M.; Marago, O. M.; Iati, M. A. Surface plasmon resonance in gold nanoparticles: a review. *J. Phys. Condens. Matter* **2017**, *29*, 203002. 10.1088/1361-648X/aa60f3

- (55) Santiago-González, B.; Vázquez-Vázquez, C.; Blanco-Varela, M. C.; Gaspar Martinho, J. M.; Ramallo-López, J. M.; Requejo, F. G.; López-Quintela, M. A. Synthesis of water-soluble gold clusters in nanosomes displaying robust photoluminescence with very large Stokes shift. *J. Colloid Interface Sci.* **2015**, *455*, 154-162. 10.1016/j.jcis.2015.05.042
- (56) Yang, T.-Q.; Peng, B.; Shan, B.-Q.; Zong, Y.-X.; Jiang, J.-G.; Wu, P.; Zhang, K. Origin of the Photoluminescence of Metal Nanoclusters: From Metal-Centered Emission to Ligand-Centered Emission. *Nanomaterials* **2020**, *10*, 261.
- (57) Rurack, K.; Spieles, M. Fluorescence Quantum Yields of a Series of Red and Near-Infrared Dyes Emitting at 600–1000 nm. *Anal. Chem.* **2011**, *83*, 1232-1242. 10.1021/ac101329h
- (58) Wu, Z.; Yao, Q.; Chai, O. J. H.; Ding, N.; Xu, W.; Zang, S.; Xie, J. Unraveling the Impact of Gold(I)–Thiolate Motifs on the Aggregation-Induced Emission of Gold Nanoclusters. *Angew. Chem. Int. Ed.* **2020**, *59*, 9934-9939. 10.1002/anie.201916675
- (59) Goswami, N.; Yao, Q.; Luo, Z.; Li, J.; Chen, T.; Xie, J. Luminescent Metal Nanoclusters with Aggregation-Induced Emission. *J. Phys. Chem. Lett.* **2016**, *7*, 962-975. 10.1021/acs.jpcclett.5b02765
- (60) Schaeffer, N.; Tan, B.; Dickinson, C.; Rosseinsky, M. J.; Laromaine, A.; McComb, D. W.; Stevens, M. M.; Wang, Y.; Petit, L.; Barentin, C.; Spiller, D. G.; Cooper, A. I.; Lévy, R. Fluorescent or not? Size-dependent fluorescence switching for polymer-stabilized gold clusters in the 1.1–1.7 nm size range. *Chem. Commun.* **2008**, 3986-3988. 10.1039/b809876j
- (61) Luo, Z.; Yuan, X.; Yu, Y.; Zhang, Q.; Leong, D. T.; Lee, J. Y.; Xie, J. From Aggregation-Induced Emission of Au(I)–Thiolate Complexes to Ultrabright Au(0)@Au(I)–Thiolate Core–Shell Nanoclusters. *J. Am. Chem. Soc.* **2012**, *134*, 16662-16670. 10.1021/ja306199p
- (62) Valeur, B.; Berberan-Santos, M. N.: *Molecular Fluorescence: Principles and Applications*; second ed.; Wiley-VCH Verlag GmbH: Weinheim, Germany 2012.
- (63) Wu, Z. K.; Jin, R. C. On the Ligand's Role in the Fluorescence of Gold Nanoclusters. *Nano Lett.* **2010**, *10* (7), 2568-2573.

- (64) Zhou, M.; Song, Y. B. Origins of Visible and Near-Infrared Emissions in [Au-25(SR)(18)]⁻ Nanoclusters. *J. Phys. Chem. Lett.* **2021**, *12*, 1514-1519. 10.1021/acs.jpcclett.1c00120
- (65) Zhou, M.; Higaki, T.; Li, Y.; Zeng, C.; Li, Q.; Sfeir, M. Y.; Jin, R. Three-Stage Evolution from Non-scalable to Scalable Optical Properties of Thiolate-Protected Gold Nanoclusters. *J. Am. Chem. Soc.* **2019**, *141*, 19754-19764. 10.1021/jacs.9b09066
- (66) Mutas, M.; Strelow, C.; Kipp, T.; Mews, A. Specific binding and internalization: an investigation of fluorescent aptamer-gold nanoclusters and cells with fluorescence lifetime imaging microscopy. *Nanoscale* **2018**, *10*, 20453-20461. 10.1039/c8nr06639f
- (67) Song, X.; Zhu, W.; Ge, X.; Li, R.; Li, S.; Chen, X.; Song, J.; Xie, J.; Chen, X.; Yang, H. A New Class of NIR-II Gold Nanocluster-Based Protein Biolabels for In Vivo Tumor-Targeted Imaging. *Angew. Chem. Int. Ed.* **2021**, *60*, 1306-1312. 10.1002/anie.202010870
- (68) Shang, L.; Dorlich, R. M.; Brandholt, S.; Schneider, R.; Trouillet, V.; Bruns, M.; Gerthsen, D.; Nienhaus, G. U. Facile preparation of water-soluble fluorescent gold nanoclusters for cellular imaging applications. *Nanoscale* **2011**, *3*, 2009-2014. 10.1039/c0nr00947d
- (69) Zhu, S.; Wang, X.; Cong, Y.; Li, L. Regulating the Optical Properties of Gold Nanoclusters for Biological Applications. *ACS Omega* **2020**, *5*, 22702-22707. 10.1021/acsomega.0c03218
- (70) Zhang, J.; Fu, Y.; Conroy, C. V.; Tang, Z.; Li, G.; Zhao, R. Y.; Wang, G. Fluorescence Intensity and Lifetime Cell Imaging with Luminescent Gold Nanoclusters. *J. Phys. Chem. C* **2012**, *116*, 26561-26569. 10.1021/jp306036y

TOC Graphic.

